International Journal of Modern Physics C
Vol. 20, No. 6 (2009) 847–867

World Scientific
www.worldscientific.com

GENERATION OF HOMOGENEOUS GRANULAR PACKINGS: CONTACT DYNAMICS SIMULATIONS AT CONSTANT PRESSURE USING FULLY PERIODIC BOUNDARIES

M. REZA SHAEBANI[*,†,§], TAMÁS UNGER[‡] and JÁNOS KERTÉSZ[†,‡]

[*] *Institute for Advanced Studies in Basic Sciences*
Zanjan 45195-1159, Iran

[†] *Department of Theoretical Physics*
Budapest University of Technology and Economics
H-1111 Budapest, Hungary

[‡] *HAS-BME Condensed Matter Research Group*
Budapest University of Technology and Economics, Budapest, Hungary

[§] *Department of Theoretical Physics*
University of Duisburg-Essen, 47048 Duisburg, Germany
[§] *shaebani@iasbs.ac.ir*
[§] *mhmdreza.shaebani@gmail.com*

Received 23 October 2008
Accepted 11 February 2009

The contact dynamics (CD) method is an efficient simulation technique of dense granular media where unilateral and frictional contact problems for a large number of rigid bodies have to be solved. In this paper, we present a modified version of the CD to generate homogeneous random packings of rigid grains. CD simulations are performed at constant external pressure, which allows the variation of the size of a periodically repeated cell. We follow the concept of the Andersen dynamics and show how it can be applied within the framework of the CD method. The main challenge here is to handle the interparticle interactions properly, which are based on constraint forces in CD. We implement the proposed algorithm, perform test simulations, and investigate the properties of the final packings.

Keywords: Granular material; nonsmooth contact dynamics; homogeneous compaction; jamming; random granular packing; constant pressure.

PACS Nos.: 45.70.-n, 45.70.Cc, 02.70.-c, 45.10.-b.

1. Introduction

Computer simulation methods have been widely employed in recent years to study the behavior of granular materials. Among the numerical techniques, discrete element methods, including *soft particle molecular dynamics* (MD),[1,2] *event-driven* (ED),[3,4] and *contact dynamics* (CD),[5–8] constitute an important class where the

material is simulated on the level of particles. In such algorithms, the trajectory of each particle is calculated as a result of interaction with other particles, confining boundaries and external fields. The differences between the discrete element methods stem from the way how interactions between the particles are treated, which leads also to different ranges of applicability.

In low-density granular systems, where interactions are mainly binary collisions, the ED method is an efficient technique. The particles are modeled as perfectly rigid and the contact duration is supposed to be zero. The handling of dense granular systems, where the frequency of collisions is large or long-lasting contacts appear, becomes problematic in ED simulations.[9,10]

In the case of dense granular media, the approach of soft particle MD is more favorable and widely used. In MD, the timestep is usually fixed and the original undeformed shapes of the particles may overlap during the dynamics. These overlaps are interpreted as elastic deformations, which generate repulsive restoring forces between the particles. Based on this interaction, which is defined in the form of a visco-elastic force law, the stiffness of the particles can be controlled. When the stiffness is increased MD simulations become slower since the timestep has to be chosen small enough so that the velocities and positions vary as smooth functions of time.

The CD method considers the grains as perfectly rigid. Therefore, no overlaps between the particles are expected and they interact with each other only at contact points. The contact forces in CD do not stem from visco-elastic force laws but are calculated in terms of constraint conditions (for more details, see Sec. 2). This method has shown its efficiency in the simulation of dense frictional systems of hard particles.

Packings of hard particles interacting with repulsive contact forces are extensively used as models of various complex many-body systems, e.g. dense granular materials,[11] glasses,[12] liquids,[13] and other random media.[14] Jamming in hard-particle packings of granular materials has been the subject of considerable interest recently.[15,16] Furthermore hard-particle packings, and especially hard-sphere packings, have inspired mathematicians and have been the source of numerous challenging theoretical problems,[17] from which many are still open.

Real systems in the laboratory and in nature contain far too large number of particles to model the whole system in computer simulations. Owing to the limited computer capacity, the simulations are often restricted to test a small mesoscopic part of a large system. Typically, the studies are focused to a local homogeneous small piece of the material inside the bulk far from the border of the system. Therefore, simulation methods are required that are able to generate and handle packings of hard particles without side effects of confining walls.

The usual simulation methods of dense systems involve confining boxes where the material is compactified by moving pistons or gravity. However, the properties of the material differ in the vicinity of walls and corners of the confining cell from those in the bulk far from the walls. The application of walls in computer simulations

leads to inhomogeneous systems due to undesired side effects (e.g. layering effect). Moreover, the structure of the packings becomes strongly anisotropic in these cases due to the orientation of walls and special direction of the compaction. For studies where such anisotropy is unwanted other type of compaction methods are needed.

In this paper, we present a compaction method where boundary effects are avoided due to exclusion of side walls. This simulation method is based on the CD algorithm where we applied the concept of the Andersen dynamics,[18] which enables us to produce homogeneous granular packings of hard particles with desired internal pressure. The compaction method involves variable volume of the simulation cell with periodic boundary conditions in all directions.

This paper is organized as follows. First, we present some basic features of CD method in Sec. 2. Then, Sec. 3 describes the equations of motion for a system of particles with variable volume. In Sec. 4, we present a modified version of CD with coupling to constant external pressure. In Sec. 5 we report the results of some test simulations. Section 6 concludes the paper.

2. Nonsmooth Contact Dynamics

CD, developed by Jean and Moreau,[6–8] is a discrete element method in the sense that the time evolution of the system is treated on the level of individual particles. Once the total force $\mathbf{F}_i$ and torque $\mathbf{T}_i$ acting on the particle i is known, the problem is reduced to the integration of Newton's equations of motion, which can be solved by numerical methods. Here we use the implicit first-order Euler scheme:

$$\mathbf{v}_i(t+\Delta t) = \mathbf{v}_i(t) + \frac{1}{m_i}\mathbf{F}_i(t+\Delta t)\Delta t\,, \tag{1}$$

$$\mathbf{r}_i(t+\Delta t) = \mathbf{r}_i(t) + \mathbf{v}_i(t+\Delta t)\Delta t\,, \tag{2}$$

which gives the change in the position $\mathbf{r}_i$ and velocity $\mathbf{v}_i$ of the center of mass of the particle with mass m_i after the timestep Δt. Δt is chosen so that the relative displacement of adjacent particles during one timestep is small compared with the particle size and with the radius of curvature of the contacting surfaces. Corresponding equations are used also for the rotational degrees of freedom, describing the time evolution of the orientation and the angular velocity $\boldsymbol{\omega}_i$ caused by the new total torque $\mathbf{T}_i(t+\Delta t)$ acting on the particle i.

The interesting part of the CD method is how the interaction between the particles are handled. For simplicity, we assume that the particles are noncohesive and dry, we exclude electrostatic and magnetic forces between them and consider only interactions via contact forces. The particles are regarded as *perfectly rigid* and the contact forces are calculated in terms of constraint conditions. Such constraints are the impenetrability and the no-slip condition, i.e. the contact force has to prevent the overlapping of the particles and the sliding of the contact surfaces. This latter condition is valid only below the Coulomb limit of static friction, which states that the tangential component of a contact force $\mathbf{R}$ cannot exceed the normal component

times the friction coefficient μ:

$$|\mathbf{R}_t| \leq \mu R_n \,. \tag{3}$$

If the friction is not strong enough to ensure the no-slip condition, the contact will be sliding and the tangential component of the contact force is given by the expression

$$\mathbf{R}_t = -\mu R_n \frac{\mathbf{v}_t^{\mathrm{rel}}}{|\mathbf{v}_t^{\mathrm{rel}}|} \,, \tag{4}$$

where $\mathbf{v}_t^{\mathrm{rel}}$ stands for the tangential component of the relative velocity between the contacting surfaces. In the CD method, the constraint conditions are imposed on the new configuration at time $t+\Delta t$, i.e. the unknown contact forces are calculated in a way that the constraints conditions are fulfilled in the new configuration.[8] This is the reason why an implicit timestepping is used.

In order to let the system evolve one step from time t to $t+\Delta t$, one has to determine the total force and torque acting on each particle, which may consist of external forces (like gravity) and contact forces from neighboring particles. Let us suppose that all the unknown contact forces are already determined except for one force between a pair of particles already in contact or with a small gap between them. Here we explain briefly how the constraint conditions help to determine the interaction between these two particles. A detailed description of the method can be found in Ref. 8.

The algorithm starts with the assumption that the contact force we are searching for is zero and checks whether this leads to an overlap of the undeformed shapes of the two particles after one timestep Δt. This is done based on the timestepping [Eq. (1)]: The external forces and other contact forces provide $F_i(t+\Delta t)$ and $T_i(t+\Delta t)$ for both particles, thus the new relative velocity of the contacting surfaces $\mathbf{v}^{\mathrm{rel,\,free}}$ can be calculated. Here we use the term *contacting surfaces* for simplicity though the two particles are not necessarily in contact. There might be a positive gap g between them, which is the length of the shortest line connecting the surfaces of the two particles (Fig. 1). We will refer to the relative velocity of the endpoints of the line as the relative velocity of the contact and denote the direction of the

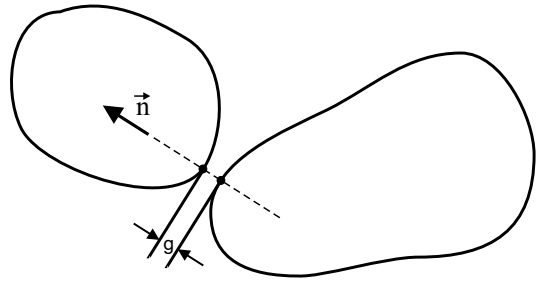

Fig. 1. Two rigid particles before a possible contact.

line by the unit vector $\mathbf{n}$. In the limit of a real contact, g is zero and $\mathbf{n}$ becomes the contact normal. Negative gap has the meaning of an overlap. The superscript *free* in $\mathbf{v}^{\mathrm{rel,\,free}}$ denotes that the relative velocity has been calculated assuming no interaction between the two particles. We use the sign convention that negative normal velocity ($\mathbf{n} \cdot \mathbf{v}^{\mathrm{rel}} < 0$) means approaching particles.

The new value of the gap (after one timestep) is estimated by the algorithm based on the current gap g and the new relative velocity $\mathbf{v}^{\mathrm{rel,\,free}}$ according to the implicit timestepping. If the new gap is positive:

$$g + \mathbf{v}^{\mathrm{rel,\,free}} \cdot \mathbf{n}\Delta t > 0 \tag{5}$$

then the zero contact force (no interaction) is accepted because no contact is formed between the two particles. However, if the estimated new gap is negative then a contact force has to be applied in order to avoid the violation of the constraint conditions. Generally, one expects the following relation between the unknown new contact force $\mathbf{R}$ and the unknown new relative velocity $\mathbf{v}^{\mathrm{rel}}$:

$$\mathbf{R} = \frac{-1}{\Delta t}\mathbf{M}(\mathbf{v}^{\mathrm{rel,\,free}} - \mathbf{v}^{\mathrm{rel}})\,, \tag{6}$$

where $\mathbf{M}$ is the mass matrix that describes the inertia of the contact, i.e. $\mathbf{M}^{-1}\mathbf{R}$ is the relative acceleration of the contacting surfaces due to the contact force $\mathbf{R}$. The mass matrix $\mathbf{M}$ depends on the shape, mass, and moment of inertia of the two particles. On the one hand, the interpenetration of the two rigid particles has to be avoided, which gives the following constraint for the normal component of $\mathbf{v}^{\mathrm{rel}}$:

$$g + \mathbf{v}^{\mathrm{rel}} \cdot \mathbf{n}\Delta t = 0\,. \tag{7}$$

On the other hand, the tangential component of $\mathbf{v}^{\mathrm{rel}}$ has to be zero in order to ensure the no-slip condition

$$\mathbf{v}_t^{\mathrm{rel}} = 0\,. \tag{8}$$

The required contact force that fulfills Eqs. (7) and (8) then reads

$$\mathbf{R} = \frac{-1}{\Delta t}\mathbf{M}\left(\frac{g}{\Delta t}\mathbf{n} + \mathbf{v}^{\mathrm{rel,\,free}}\right)\,. \tag{9}$$

This contact force is acceptable only if it fulfills the Coulomb condition [Eq. (3)]. Otherwise we cannot exploit the nonslip contact assumption. In this case, $\mathbf{v}_t^{\mathrm{rel}}$ is not zero, the contact slides and the contact force has to be recalculated. Equations (6) and (7) then provide

$$\mathbf{R} = \frac{-1}{\Delta t}\mathbf{M}\left(\frac{g}{\Delta t}\mathbf{n} - \mathbf{v}_t^{\mathrm{rel}} + \mathbf{v}^{\mathrm{rel,\,free}}\right)\,, \tag{10}$$

where the number of unknowns (components of $\mathbf{R}$ and $\mathbf{v}_t^{\mathrm{rel}}$) exceeds the number of equations. In order to determine the contact force $\mathbf{R}$, one has to solve Eq. (10) together with Eq. (4).

It is recommended to use $g^{\mathrm{pos}} = \max(g, 0)$ instead of g in Eqs. (9) and (10). The gap size g should always be nonnegative and using g^{pos} apparently makes no

difference.[7] However, due to the inaccuracy of the calculations small overlaps can be created between neighboring particles. If g instead of g^{pos} is used then these overlaps are eliminated in the next timestep by imposing larger repulsive contact forces to satisfy Eq. (7), which pumps kinetic energy into the system. Using g^{pos} instead of g eliminates this artifact on the cost that an already existing overlap is not removed (which then serves to check the inaccuracies of the simulation[19]), only its further growth is prevented. Regarding the above-mentioned points, we rewrite Eqs. (9) and (10) as

$$\mathbf{R} = \frac{-1}{\Delta t}\mathbf{M}\left(\frac{g^{\mathrm{pos}}}{\Delta t}\mathbf{n} + \mathbf{v}^{\mathrm{rel,\,free}}\right) \quad \text{and} \tag{11}$$

$$\mathbf{R} = \frac{-1}{\Delta t}\mathbf{M}\left(\frac{g^{\mathrm{pos}}}{\Delta t}\mathbf{n} - \mathbf{v}_t^{\mathrm{rel}} + \mathbf{v}^{\mathrm{rel,\,free}}\right). \tag{12}$$

A flowchart of the single contact force calculation is given in Fig. 2. So far we have explained only how the CD algorithm determines a single existing or incipient contact, based on the assumption that all the surrounding contact forces are known. However, in a dense granular media, many particles contact simultaneously and form a contact network. In this case, a contact force cannot be evaluated locally, since it depends on the adjacent contact forces which are also unknown. To find a globally consistent force network at each timestep, an *iterative scheme* is applied in CD.

At each iteration step, all contacts are chosen one by one and the force at the contact is updated according to the scheme shown in Fig. 2. The update is sequential, i.e. the freshly updated contact force is stored immediately as the current force and then a new contact is chosen for the next update.

After one iteration step, constraint conditions are not necessarily fulfilled for each contact. In order to find a global solution, the iteration process has to be repeated several times until the resulting force network converges. The convergence of the iteration process is smooth, i.e. the precision of the solution increases with the number of iterations N_I. Higher N_I provides more precise solution but also requires more computational effort. The CD method can be used with a constant number of iterations in subsequent timesteps[19,8] or with a convergence criterion that prescribes a given precision to the force calculation.[6–8] In this latter case, the number of iterations N_I varies from timestep to timestep.

After the new force network is determined with a prescribed precision, the system evolves at the end of the timestep according to the timestepping scheme described at the beginning of this section. It is important to note that choosing small N_I and/or large timestep causes systematic errors of the force calculation, which lead to a spurious soft particle behavior[19] in spite of the original assumption of perfect rigidity.

To conclude this section, we present briefly the scheme of the solver:

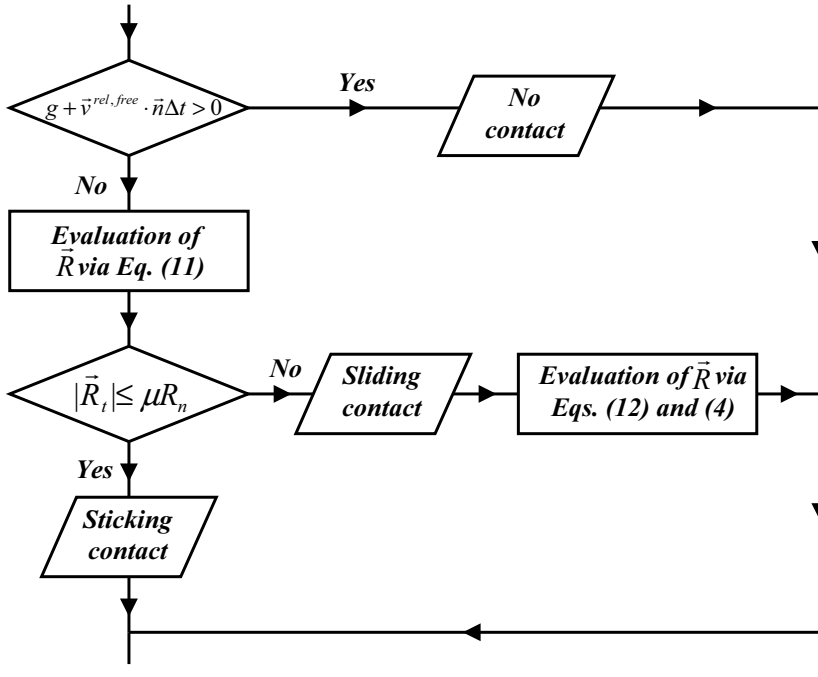

Fig. 2. The flowchart of the force calculation of a single contact in contact dynamics.

$t := t + \Delta t$ (timestep)
Evaluating the gap g for all contacts
$N_I := N_I + 1$ (iteration)
$k := k + 1$ (contact index)
Evaluating $\mathbf{v}_k^{\text{rel, free}}$ then $\mathbf{R}_k$ (according to the flowchart in Fig. 2)
Convergence test for contact forces
Timestepping for velocities and positions of all particles (using Eqs. (1) and (2))

3. The Equations of Motion at Constant External Pressure

In the simulation of granular materials, it is often desirable to investigate systems, which are not surrounded by walls and to apply periodic boundary conditions in all directions. It is a nice feature of periodic boundary conditions that they make points of the space equivalent, the boundary effects are eliminated. That way the bulk properties of the material can be studied more easily. However, the application of an external pressure becomes problematic since the total volume is fixed and the system cannot be compressed by pistons or moving walls.

In order to overcome this problem, but at the same time keep the advantageous periodic boundaries, Andersen[18] proposed a method for MD simulations. Here, we recall his method briefly as its basic ideas will be used later on in this paper.

According to the Andersen method, the boundaries are still periodically connected in all directions and no walls are present, but the volume of the system is a dynamical variable, which evolves in time driven by constant external pressure. When a system of N atoms is compressed or expanded it is done in an isotropic and homogeneous way: The distances between the atoms are rescaled by the same factor regardless of the relative or absolute positions.

Let us give the equations of motion of a system with particle positions $\mathbf{r}_1, \mathbf{r}_2, \ldots, \mathbf{r}_N$ in a D-dimensional cubic volume V ($D = 2$, 3 and each component of $\mathbf{r}_i$ is between 0 and $V^{1/\mathrm{D}}$):

$$\frac{d\mathbf{r}_i(t)}{dt} = \frac{\mathbf{p}_i(t)}{m_i} + \frac{1}{D}\mathbf{r}_i(t)\frac{d\ln V(t)}{dt}\,, \tag{13}$$

$$\frac{d\mathbf{p}_i(t)}{dt} = \mathbf{F}_i(t) - \frac{1}{D}\mathbf{p}_i(t)\frac{d\ln V(t)}{dt}, \tag{14}$$

$$\frac{M_\mathrm{v} d^2V(t)}{dt^2} = P_\mathrm{in}(t) - P_\mathrm{ext} = \Delta P(t)\,. \tag{15}$$

Equation (13) describes the change in the position $\mathbf{r}_i$. The first term on the right is the usual one, the momentum $\mathbf{p}_i$ divided by the mass of the ith particle. The last term is the extension by the Andersen method that rescales the position according to the relative volume change.

Equation (14) provides the time evolution of the momentum due to two terms. The first one is the usual total force $\mathbf{F}_i$ acting on the ith particle, which originates from the interaction with other particles and/or from external fields. The additional term leads to further acceleration of the particle if the volume is changing. For example, if the system is compressed the kinetic energy of the particles is increased due to the work done by the compression. The energy input is achieved by rescaling all particle momenta regardless of their positions. This is in contrast to usual pistons where the energy enters at the boundary.

Equation (15) can be interpreted as Newton's second law that governs the change of the volume. It describes the time evolution of an imaginary piston, which has the inertia parameter M_v and is driven by the generalized force $\Delta P(t) = P_\mathrm{in}(t) - P_\mathrm{ext}$. This latter is the pressure difference between the constant external pressure P_ext and the internal pressure of the system $P_\mathrm{in}(t)$. The pressure difference $\Delta P(t)$ drives the system toward the external pressure, the sensitivity of the system to this driving force is controlled by the inertia parameter M_v.

In the limit of infinite inertia $M_\mathrm{v} \to \infty$ together with the initial condition $dV(t_0)/dt = 0$, the volume of the system remains constant and Eqs. (13) and (14) correspond to the usual Newtonian dynamics of the particles.

In order to get more insight into the Andersen dynamics, let us consider a simple example of a system of noninteracting particles with all $\mathbf{F}_i(t) = 0$. Initially, the velocities and the volume velocity $dV(t_0)/dt$ are set to zero. Because the internal pressure P_in is zero the system with finite inertia M_v and under external pressure

$P_{\text{ext}} > 0$ will start contracting according to Eq. (15). The acceleration of the particles [Eq. (14)] remains zero during the time evolution; one might say that the particles are standing there all the time. However, the distances between them are decreasing because of the contraction of the "world" around them. This is caused by the second term on the right-hand side of Eq. (13) while the first term remains zero.

This suggests the picture of an imaginary background membrane that contracts or dilates homogeneously together with the volume and carries the particles along. The velocity of this background at position $\mathbf{r}_i$ is given by $\lambda(t)\mathbf{r}_i$ where λ is the dilation rate defined by the rate of the relative change in the system size L:

$$\lambda(t) \equiv \frac{\dot{L}(t)}{L(t)} = \frac{1}{D}\frac{d\ln V(t)}{dt}\,, \tag{16}$$

and D is the dimension of the system. Then the right-hand side of Eq. (13) can be interpreted as the sum of two velocities: the second one is the velocity of the background at the position of the particle and the first one is the intrinsic velocity of the particle measured compared with the background. The sum of these two forces gives the changing rate of the absolute position $\mathbf{r}_i$. In the remainder of the paper, the velocity $\mathbf{v}_i$ will refer always to the intrinsic velocity. We rewrite Eq. (13) in the following form:

$$\frac{d\mathbf{r}_i(t)}{dt} = \mathbf{v}_i(t) + \lambda(t)\mathbf{r}_i(t)\,. \tag{17}$$

Next we turn to the modeling of granular systems. Our goal is to achieve static granular packings that are compressed from a loose gas-like state. Here again it is advantageous to exclude confining walls and in order to apply pressure and achieve contraction of the volume we will use the concept of the Andersen method. However, the equations of motion will be slightly changed in order to make them suit better to our goals.

In granular materials, the interactions between the particles are dissipative. When the material is poured into a container or is compressed by a piston, the particles gain kinetic energy due to the work done by gravity or the piston. All this energy has to be dissipated (turned into heat) by the interactions between the particles before the material can settle into a static dense packing of the particles. This relaxation process requires a massive computational effort when large packings are modeled in computer simulations. One encounters the same problem if the Andersen dynamics is applied straight to granular systems. The role of the second term on the right-hand side of Eq. (14) is to conserve the total energy of the system by taking into account the energy gain of the particles due to compaction. The relaxation time can be reduced if this term is omitted, because then the total amount of energy pumped into the system is reduced. In this case, the particles are accelerated only by the forces $\mathbf{F}_i$ but they receive no additional energy due to the decreasing volume. Thus, the following equation will be applied for granular

compaction here

$$\frac{d\mathbf{v}_i(t)}{dt} = \frac{1}{m_i}\mathbf{F}_i(t)\,, \tag{18}$$

which results in a more effective relaxation rather than Eq. (14). This change is advantageous also from the point of view of momentum conservation. If the system is compactified by using Eq. (14) from an initial condition where the total momentum of the particles is nonzero, then this momentum will be increased inverse proportionally to the size of the system L. Thus, the total momentum, e.g. due to initial random fluctuations, is magnified, which can lead to nonnegligible overall rigid body motion of the final static packing. This is in contrast to Eq. (18), which provides momentum conservation in the absence of external fields.

We note that neglecting the term in Eq. (14) leads to an artificial dynamics in the sense that the energy corresponding to the work of the compaction is not delivered to the particles. However, our main goal here is to produce a static configuration of grains and contact forces that can be used for further studies, thus we are not interested in that part of the dynamics, where compaction rate is significant and the neglected term makes a difference.

Concerning the equation that describes the time evolution of the system size, we find it more convenient to control λ instead of dV/dt. This is actually not an important change and leads to very similar dynamics. Our third equation reads

$$M_\lambda \frac{d\lambda(t)}{dt} = \Delta P(t)\,. \tag{19}$$

The equations of motion (17), (18), and (19) describe an effective compaction dynamics for granular systems, they are able to provide static packings under the desired pressure P_{ext} and if they are restricted to the limit of $M_\lambda \to \infty$ we receive back the classical Newtonian dynamics.

We note that the force scale in our systems of rigid particles is determined by the external pressure as there is no intrinsic force scale. Taking larger value of P_{ext} leads in principle to the same compaction dynamics (apart from rescaling time, velocities, and forces). Consequently, the same final packing-configuration is expected, independently of the external pressure. Of course, the value of P_{ext} does matter if an intrinsic force scale is present, e.g. when cohesion between the particles is incorporated. In such cases, the final packing will strongly depend on the applied external pressure.

In order to close the equations we need to define interactions between the particles. The interparticle forces provide $\mathbf{F}_i$ in Eq. (18) and they are also needed to evaluate the inner pressure P_{in}.

The stress tensor $\sigma_{\alpha\beta}$ is not *a priori* spherical in granular materials. The average $\sigma_{\alpha\beta}$ of the system is determined by the interparticle forces[20] and the particle velocities as

$$\sigma_{\alpha\beta} = \frac{1}{V}\left(\sum_{k=1}^{N_c} F_{k,\alpha} l_{k,\beta} + \sum_{i=1}^{N} m_i v_{i,\alpha} v_{i,\beta}\right)\,, \tag{20}$$

where N and N_c denote the number of particles and the number of contacts, respectively. If two contacting particles at contact k are labeled by 1 and 2, then $\mathbf{F}_k$ is the force exerted on particle 2 by particle 1, and the vector $\mathbf{l}_k$ is pointing from the center of mass of particle 1 to that of particle 2 where periodic boundary conditions and nearest image neighbors are taken into account. Thus, l_k is the minimum distance between particles 1 and 2:

$$l_k = |\mathbf{l}_k| = \min |\mathbf{r}_2 - \mathbf{r}_1 + V^{1/3}\mathbf{a}| \,, \tag{21}$$

where $\mathbf{a}$ is an integer-component translation vector. The inner pressure is then given by the trace of the stress tensor divided by the dimension of the system

$$P_{\text{in}} = \frac{1}{\text{DV}} \left[\sum_{k=1}^{N_c} \mathbf{F}_k \cdot \mathbf{l}_k + \sum_{i=1}^{N} m_i \mathbf{v}_i \cdot \mathbf{v}_i \right] , \tag{22}$$

which has the meaning of an average normal stress.

The implementation of the above method in computer simulations is straightforward if the interparticle forces are functions of the positions and velocities of the particles, e.g. in soft particle MD simulations. The implementation is less trivial for the case of the CD method where interparticle forces are constraint forces. We devote the next section to this problem.

4. Contact Dynamics with Coupling to a Constant External Pressure

In this section, we present a modified version of the CD algorithm, which enables us to perform CD simulations at constant external pressure. According to Sec. 3, let us suppose that the system is subjected to a constant external pressure P_{ext} and its time evolution is given by Eqs. (17), (18), and (19).

Here we will follow the description of the CD method given in Sec. 2 and discuss the required modifications. Once the force calculation process is completed, the implicit Euler integration can proceed one timestep further. Now the timestepping has to involve also the equations of motion of the system size. By discretizing the Eqs. (16) and (19) in the same implicit manner as for the particles [Eqs. (1) and (2)] we obtain the new values of the system size L and the dilation rate λ:

$$\lambda(t + \Delta t) = \lambda(t) + \frac{\Delta P(t + \Delta t)}{M_\lambda} \Delta t \,, \tag{23}$$

$$L(t + \Delta t) = L(t)[1 + \lambda(t + \Delta t)\Delta t] \tag{24}$$

where the "velocity" $\lambda(t)$ and the "position" $L(t)$ are updated by the new "force" $\Delta P(t + \Delta t)$ and by the new "velocity" $\lambda(t + \Delta t)$, respectively.

The discretized equations governing the translational degrees of freedom of the particles [Eqs. (1) and (2)] are rewritten according to Eqs. (17) and (18) in the

following form:

$$\mathbf{v}_i(t+\Delta t) = \mathbf{v}_i(t) + \frac{1}{m_i}\mathbf{F}_i(t+\Delta t)\Delta t \quad \text{and} \tag{25}$$

$$\mathbf{r}_i(t+\Delta t) = \mathbf{r}_i(t)[1+\lambda(t+\Delta t)\Delta t] + \mathbf{v}_i(t+\Delta t)\Delta t\,. \tag{26}$$

The timestepping for the rotational degrees of freedom remains unchanged because the dilation (contraction) of the system has no direct effect on the rotation of the particles.

In the CD method, as we explained in Sec. 2 the particles are perfectly rigid and are interacting with constraint forces, i.e. those forces are chosen between contacting particles that are needed to fulfill the constraint conditions. For example, the contact force has to prevent the interpenetration of the contacting surfaces.

If a constant external pressure is used then the calculation of the constraint forces has to be reconsidered because the relative velocity of the contacting surfaces is influenced by the variable volume. When the system is dilating or contracting, particles gain additional relative velocities compared with each other. For a pair of particles, this velocity is $\lambda\mathbf{l}$ where $\mathbf{l}$ is the vector connecting the two centers of mass. The same change appears in the relative velocity of the contacting surfaces as the size of the particles is kept fixed. If this change led to interpenetration then it has to be compensated by a larger contact force. It may also happen that existing contacts open up due to expansion of the system resulting in zero interaction force for those pair of particles.

In the calculation of a single contact force, the relative velocity $\lambda\mathbf{l}$ (i.e. the contribution of the changing system size) has to be added to $\mathbf{v}^{\mathrm{rel,\,free}}$. The new relative velocity of the contact assuming no interaction between the two particles $\mathbf{v}^{\mathrm{rel,\,free}}$ is calculated here in the same way as in Sec. 2, i.e. based on the intrinsic velocities of the particles. Thus, the effect of the dilation/contraction of the system is not taken into account in $\mathbf{v}^{\mathrm{rel,\,free}}$. Therefore, one has to replace $\mathbf{v}^{\mathrm{rel,\,free}}$ with $(\mathbf{v}^{\mathrm{rel,\,free}} + \lambda\mathbf{l})$ in all equations of Sec. 2 in order to impose the constraint conditions properly. Let us first suppose that the system has infinite inertia ($M_\lambda = \infty$) thus the dilation rate λ is constant. In this case the modified equations of the force update (containing already the term $\mathbf{v}^{\mathrm{rel,\,free}} + \lambda\mathbf{l}$) provide the right constraint forces at the end of the iteration process. These forces will alter the relative velocity $(\mathbf{v}^{\mathrm{rel,\,free}} + \lambda\mathbf{l})$ in such a way that the prescribed constrain conditions will be fulfilled in the new configuration at $t + \Delta t$.

More consideration is needed if finite inertia M_λ is used and the dilation rate λ is time-dependent. The problem is that in order to calculate the proper contact force one has to know the new dilation rate. The new dilation rate, however, depends on the new value of the inner pressure [Eq. (23)], which, in turn, depends on the new value of the contact forces. This problem can be solved by incorporating λ and P_{in} into the iteration process. Instead of using the old values $\lambda(t)$ and $P_{\mathrm{in}}(t)$ during the iteration, we always use the expected values λ^* and P^*_{in}. These represent our best guess for the new dilation rate $\lambda(t+\Delta t)$ and for the new inner pressure $P_{\mathrm{in}}(t+\Delta t)$.

P^*_{in} is defined based on the current values of the contact forces $\mathbf{F}^*_k$ during the force iteration. Whenever a contact force is updated, we recalculate the expected inner pressure P^*_{in}. With the help of the current contact forces $\mathbf{F}^*_k$ we can determine the total forces acting on the particles and then, following Eq. (25) we also obtain the expected new velocities of the particles $\mathbf{v}^*_i$. The expected inner pressure, according to Eq. (22), then reads

$$P^*_{\text{in}} = \frac{1}{\text{DV}} \left[\sum_{k=1}^{N_c} \mathbf{F}^*_k \cdot \mathbf{l}_k + \sum_{i=1}^{N} m_i \mathbf{v}^*_i \cdot \mathbf{v}^*_i \right] . \tag{27}$$

Of course, there is no need to recalculate all the terms in Eq. (27) in order to update P^*_{in}. When the force at a single contact is changed it affects only three terms: one due to the force itself and two due to the velocities of the contacting particles. In order to save computational time, only the differences in these three terms have to be taken into account when P^*_{in} is updated. Following Eq. (23), we also obtain the corresponding value of the expected dilation rate:

$$\lambda^* = \lambda(t) + \frac{P^*_{\text{in}} - P_{\text{ext}}}{M_\lambda} \Delta t \tag{28}$$

In this way, λ^* and P^*_{in} are updated many times between two consecutive timesteps (in fact they are updated $N_I N_c$ times) but in turn λ^* and P^*_{in} are always consistent with the current system of the contact forces. At the end of the iteration process P^*_{in} and λ^* provide not just an approximation of the new inner pressure and new dilation rate but they are equal to $P_{\text{in}}(t + \Delta t)$ and $\lambda(t + \Delta t)$, respectively.

To complete the algorithm, we list here also the equations that are used for the force calculation of a single contact. The inequality (5) is replaced by

$$g + (\mathbf{v}^{\text{rel, free}} + \lambda^* \mathbf{l}) \cdot \mathbf{n} \Delta t > 0 \,, \tag{29}$$

i.e. there is no interaction between the two particles if the inequality is satisfied. Otherwise we need a contact force. The force, previously given by Eq. (11), that is required by a sticking contact is

$$\mathbf{R} = \frac{-1}{\Delta t} \mathbf{M} \left(\frac{g^{\text{pos}}}{\Delta t} \mathbf{n} + \lambda^* \mathbf{l} + \mathbf{v}^{\text{rel, free}} \right) . \tag{30}$$

This force again has to be recalculated according to a sliding contact if $\mathbf{R}$ in Eq. (30) violates the Coulomb condition:

$$\mathbf{R} = \frac{-1}{\Delta t} \mathbf{M} \left(\frac{g^{\text{pos}}}{\Delta t} \mathbf{n} - \mathbf{v}^{\text{rel}}_t + \lambda^* \mathbf{l} + \mathbf{v}^{\text{rel, free}} \right) , \tag{31}$$

which replaces the original Eq. (12).

Except the above changes, the CD algorithm remains the same. In each timestep, the same iteration process is applied in order to reach convergence of the contact forces. After the iteration process we apply Eqs. (23)–(26) to complete the timestep.

The scheme of the solver for the modified version of CD can be presented as

- $t = t + \Delta t$ (timestep)
- Evaluating the gap g for all contacts
  - $N_I = N_I + 1$ (iteration)
    - $k = k + 1$ (contact index)
    - Evaluating $\mathbf{v}_k^{\text{rel, free}}$
    - Evaluating $\mathbf{R}_k$ [using Eqs. (30) and (31)]
    - Evaluating P_{in}^* [Eq. (27)] then λ^* [Eq. (28)]
  - Convergence test for contact forces
  - Timestepping for the dilation rate and the system size [using Eqs. (23) and (24)]
  - Timestepping for velocities and positions of all particles [using Eqs. (25) and (26)]

In the next section, we will present some simulations with the above method. We will test the algorithm and analyze the properties of the resulting packings.

As an alternative to this fully implicit method, we considered another possibility to discretize Eqs. (16)–(19) in the spirit of the CD and, at the same time, impose the constraint conditions on the new configuration. The main difference is that the new value of the inner pressure $P_{\text{in}}(t+\Delta t)$ is determined based on the old velocities $\mathbf{v}_i(t)$ and not on the new ones $\mathbf{v}_i(t + \Delta t)$, while the contribution of the forces are taken into account in the same way, i.e. the new contact forces $\mathbf{F}_k(t + \Delta t)$ are used in Eq. (22). Therefore, this version of the method is only partially implicit, however, the constraint conditions and the force calculation [Eqs. (29)–(31)] can be applied in the same way. Only, the expected values λ^* and P_{in}^* has to be changed consistently with the new pressure $P_{\text{in}}(t + \Delta t)$:

$$P_{\text{in}}^* = \frac{1}{\text{DV}} \left[\sum_{k=1}^{N_c} \mathbf{F}_k^* \cdot \mathbf{l}_k + \sum_{i=1}^{N} m_i \mathbf{v}_i(t) \cdot \mathbf{v}_i(t) \right] \tag{32}$$

and then this modified P_{in}^* is used to determine the expected dilation rate λ^* with the help of Eq. (28). Again here, P_{in}^* and λ^* are calculated a new after each force update during the iteration process and their last values equal the new pressure $P_{\text{in}}(t + \Delta t)$ and the new dilation rate $\lambda(t + \Delta t)$.

We implemented and tested this second version of the method and found that the constraint conditions are handled here also with the same level of accuracy. Although the second method is perhaps less transparent than the fully implicit version, for practical applications it seems to be more useful. First, the second version of the method is easier to implement into a program code, second, it turned out to be faster by 25% in our test simulations. The improvement of the computational speed originates from the smaller number of the operations. One does not have to handle the expected particle velocities $\mathbf{v}_i^*$ and the recalculation of P_{in}^* is more simple as the change of a contact force $\mathbf{F}_k^*$ affects only one term in Eq. (32). We note that here the distinction "partially implicit" and "fully implicit" refer only to the difference, whether the velocities are or are not included in the iteration process.

5. Numerical Results

We perform numerical simulations using the CD algorithm with the fully implicit constant pressure scheme of Sec. 4. This algorithm has been used to study mechanical properties of granular packings in response to local perturbations.[21,22,26] Here, the main goal is to show that the algorithm works indeed in practical applications and to test the method from several aspects. We investigate how the simulation parameters influence the required CPU time and the accuracy of the simulation. Such parameters are the external pressure P_{ext}, the inertia parameter M_λ, and the computational parameters, such as the number of iterations per timestep N_I and the length of the timestep Δt. We also analyze the properties of the resulting packings.

Here, we report only simulations of two-dimensional systems of disks, where the behavior is very similar to that we found for spherical particles in three-dimensional systems. Length parameters, the time, and the two-dimensional mass density of the particles are measured in arbitrary units of l_0, t_0, and ρ_0, respectively. The samples are polydisperse and the disk radii are distributed uniformly between 0.8 and 1.2, thus the average grain radius is 1. The material of the grains has unit density and the masses of the disks are proportional to their areas. In this section, we have one reference system that contains 100 disks. The interparticle friction coefficient is set to 0.5. The value of other parameters are $N_I = 100$, $\Delta t = 0.01$, $P_{\text{ext}} = 1$ (this latter is expressed in units of $\rho_0 l_0^2/t_0^2$), and the inertia $M_\lambda = 100$ (in units of $\rho_0 l_0^2$). Throughout this section, we either use these reference parameters or the modified values will be given explicitly. Usually, we will vary only one parameter to check its effect while other parameters are kept fixed at their reference values.

In each simulation, we start with a dilute sample of nonoverlapping rigid disks randomly distributed in a two-dimensional square-shaped cell [Fig. 3(a)]. No confining walls are used according to the boundary conditions specified in Sec. 4. Gravity and the initial dilation rate are set to zero. Owing to imposing a constant external pressure, the dilute system starts shrinking. As the size of the cell decreases, particles collide, dissipate energy and after a while a contact force network is formed between touching particles in order to avoid interpenetrations. The contact forces build up the inner pressure P_{in}, which inhibits further contraction of the system. Finally, a static configuration is reached in which P_{in} equals P_{ext} and mechanical equilibrium is provided for each particle [Fig. 3(b)]. Technically, we finish the simulation when the system is close enough to the equilibrium state: We apply a convergence threshold for the mean velocity v_{mean} and mean acceleration a_{mean} of the particles (which are measured in units l_0/t_0 and l_0/t_0^2, respectively). Only if both v_{mean} and a_{mean} become smaller than the threshold 10^{-10} we regard the system as relaxed and stop the simulation.

The typical time evolution can be seen in Fig. 4 where we show the compaction process in the case of the reference system. Figure 4(left) implies that the magnitude of λ grows linearly in the beginning when the inner pressure is close to zero. The

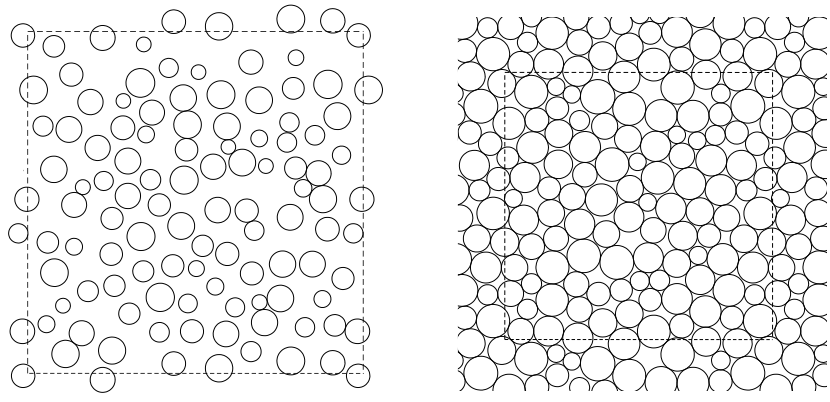

(a) (b)

Fig. 3. Schematic picture of a two-dimensional granular system controlled by a constant external pressure: (a) the initial gas state, and (b) the final homogeneous packing. The dashed lines mark periodic boundaries.

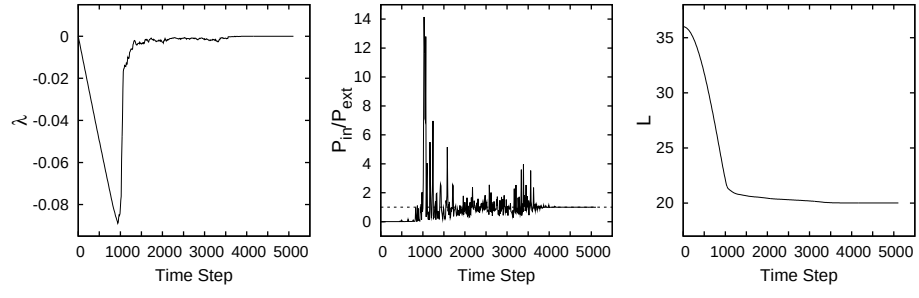

Fig. 4. Typical time evolution of the dilation rate λ (left), the inner pressure $P_{\rm in}$ (middle), and the system size L (right) during the compression of a two-dimensional polydisperse sample. The data shown here were recorded in the reference system specified in the text.

negative value of the dilation rate indicates contraction, which becomes slower after the particles build up the inner pressure [Fig. 4(middle)]. The fluctuations in $P_{\rm in}$ are due to collisions of the particles. In the final stage of the compression, λ goes to zero, $P_{\rm in}$ converges to the external pressure, and the size of the system reaches its final value [Fig. 4(right)].

Next we investigate how the required CPU time of the simulation is affected by the various parameters. All simulations are performed with a processor Intel(R) Core(TM)2 CPU T7200 @ 2.00 GHz and the CPU time is measured in seconds. Figure 5 reveals that the variation of $P_{\rm ext}$, Δt, N_I, and M_λ have direct influence on the required CPU time. The final packing is achieved with less computational expenses if larger $P_{\rm ext}$, larger Δt, or smaller N_I is used. The role of system inertia M_λ is more complicated. M_λ reflects the sensitivity of the system to the pressure difference $P_{\rm in} - P_{\rm ext}$. If the level of the sensitivity is too small or too large, the

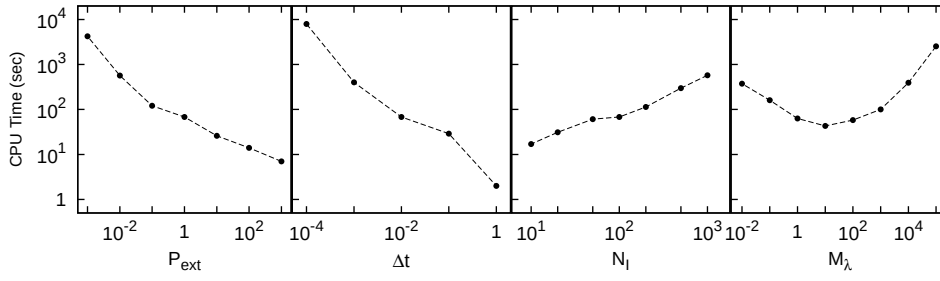

Fig. 5. CPU time vs the simulation parameters.

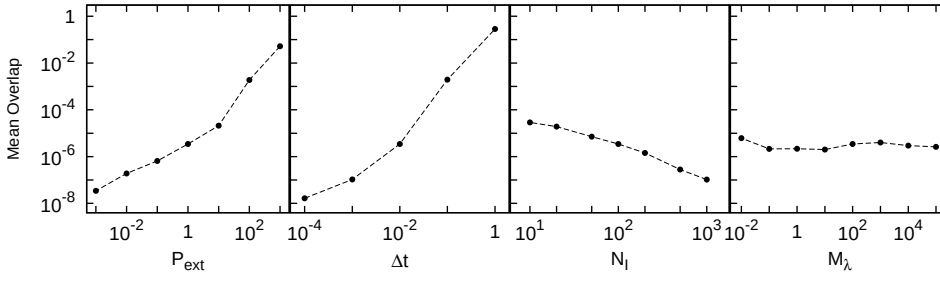

Fig. 6. Mean overlap in terms of the simulation parameters.

simulation becomes inefficient. It is advantageous to choose the inertia M_λ near to its optimal value, which depends on the specific system (e.g. on the number and mass of the particles).[23]

Regarding the efficiency of the computer simulation, not only the computational expenses play an important role but the accuracy of the simulation is also essential. Here we use the overlaps of the particles as a measure of the inaccuracy of the simulation (see Sec. 2). In an ideal case, there would be no overlaps between perfectly rigid particles. Figure 6 shows the mean overlaps measured in the final packings. It can be seen for the parameters P_{ext}, Δt, and N_I that the reduction of the computational expenses at the same time leads also to the reduction of the accuracy of the simulation. In Fig. 7(left), we plot the CPU time vs the mean overlap for these three parameters. The data points collapse approximately on the same master curve, which tells us that the computational expenses are determined basically by the desired accuracy; smaller errors require more computations. The efficiency of the simulation is approximately independent of the parameters P_{ext}, Δt, and N_I. The situation is, however, different for the inertia of the system M_λ. First, it has relatively small effect on the accuracy of the simulation (Fig. 6). Variation of M_λ by seven orders of magnitude could hardly change the mean overlap of the particles. Second, M_λ affects strongly the efficiency of the simulation, which is shown clearly by Fig. 7(right). If M_λ is varied then larger computational expense is not necessarily accompanied with smaller errors. In fact, in the whole range of M_λ

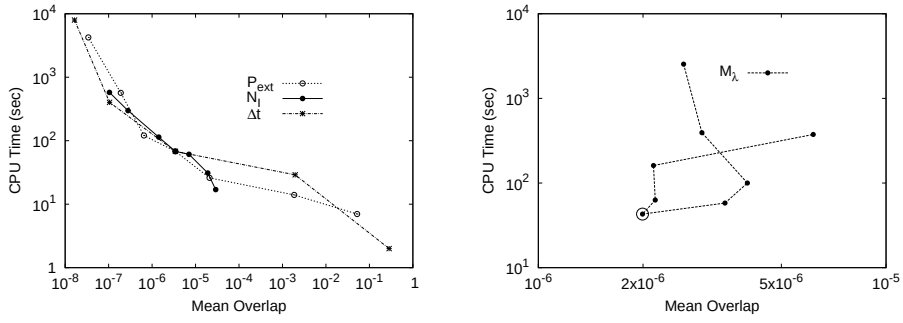

Fig. 7. CPU time in terms of the mean overlap. The different curves are obtained by the variation of different parameters according to Figs. 5 and 6. These parameters are the external pressure P_{ext}, the number of iterations per timestep N_I, the length of the timestep Δt (left), and the inertia of the system M_λ (right). The open circle on the right indicates the most efficient simulation we could achieve by controlling the inertia M_λ.

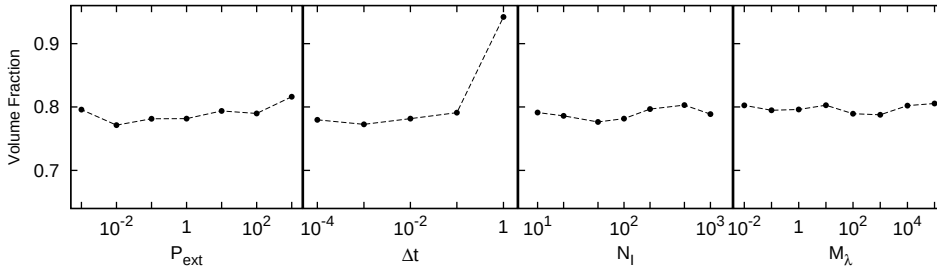

Fig. 8. Volume fraction vs the simulation parameters.

studied here, the fastest simulation turned out to be the most accurate one [open circle in Fig. 7(right)].

Next we turn to the question whether the parameters of the simulation used in the compaction process influence the physical properties of the final packing. There are many ways to characterize static packings of disks. Here we test only one quantity, the frequently used volume fraction. The volume fraction gives the ratio between the total volume (total area in two dimensions) of grains and the volume (area) of the system. Figure 8 shows the volume fraction of the same packings that were studied already in Fig. 6. It can be seen that the volume fraction remains approximately unchanged under the variation of the four parameters P_{ext}, N_I, Δt, and M_λ. This is except for one data point for large timestep Δt, where the simulation is very inaccurate. The corresponding mean overlap (Fig. 6) is comparable to the typical size of the particles which is the reason, why the volume fraction appears to be much larger.

Finally, we investigate the inner structure of the resulting random packings. For that, we study larger samples with $N = 1000$ particles; otherwise, the default parameters are used during the compaction. To suppress random fluctuations, we

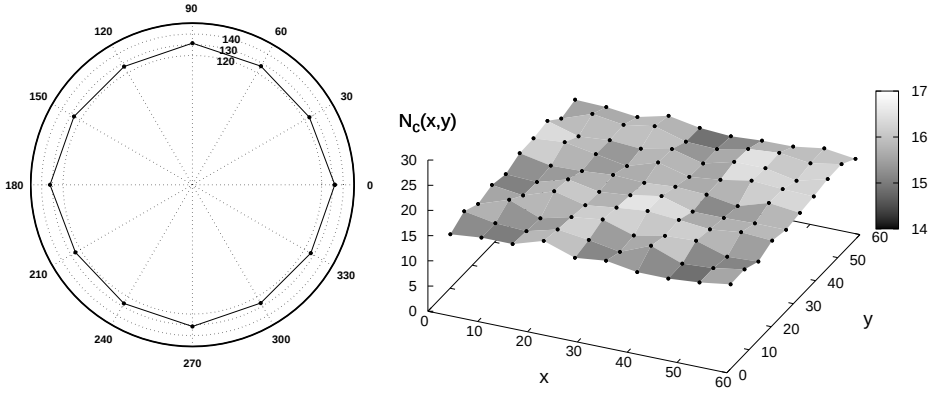

Fig. 9. (left) The angular distribution of the contacts. The number of contacts is plotted in terms of the direction of their normal vectors. (right) Spatial distribution of the contacts. The system contains $N = 1000$ disks in both figures.

produce five different systems and all quantities reported hereafter represent average values over these systems. In Fig. 9(left) we study the angular distribution of the contact normals and find that it is very close to uniform. However, there is a small but definite deviation (around 3%): the density of the contact normals are slightly larger parallel to the periodic boundaries. In this sense, the packing is not completely isotropic. Although the effect is very small, the orientation of the boundaries can be observed also in such local quantities like the direction of the contacts.

In connection to the question of the isotropy, we checked also the global stress tensor σ. In the original frame σ reads

$$\sigma = \begin{pmatrix} 1.00909 & -0.01334 \\ -0.01332 & 0.99091 \end{pmatrix} . \tag{33}$$

This stress is isotropic with good approximation. The diagonal entries are close to 1 which equals P_{ext} while the off-diagonal elements are approximately zero. Compared with the unit matrix, the elements deviate around 1% of P_{ext}.

The final packings are expected to be homogeneous as all points of the space are handled equivalently by the compaction method. Apart from random fluctuations, we do not observe any inhomogeneity in our test systems. As an example, we show the spatial distribution of the contacts in Fig. 9(right), where the density is approximately constant.

6. Concluding Remarks

In this work, we have proposed and tested a simulation method to produce homogeneous random packings in the absence of confining walls. We combined the CD algorithm with a modified version of the Andersen method to perform constant pressure simulations of granular systems. Our main concern was to

discuss how constraint conditions can be applied to determine the interaction between the particles in an Andersen-type of dynamics. We have presented the results of some numerical tests and discussed the effect of the main parameters on the efficiency of the simulations and on the physical properties of the final packings.

We restricted our study to the simple case where we allow only spherical strain of the system in order to achieve the desired pressure. However, the method can be generalized to apply other type of constraints to the stress tensor and, consequently, to allow more general strain deformations where shape as well as size of the simulation cell can be varied.[24,25]

Acknowledgments

The authors acknowledge support by grants Nos. OTKA T049403, OTKA PD073172, and by the Bolyai Janos Scholarship of the Hungarian Academy of Sciences.

References

1. P. A. Cundall and O. D. L. Strack, *Géotechnique* **29**, 47 (1979).
2. L. E. Silbert *et al.*, *Phys. Rev. E* **65**, 031304 (2002).
3. D. C. Rapaport, *J. Comp. Phys.* **34**, 184 (1980).
4. O. R. Walton and R. L. Braun, *J. Rheol.* **30**, 949 (1986).
5. M. Jean and J. J. Moreau, *Unilaterality and Dry Friction in the Dynamics of Rigid Body Collections — Proc. Contact Mechanics Intern. Symposium*, ed. A. Curnier (Presses Polytechniques et Universitaires Romandes, 1992), p. 31.
6. J. J. Moreau, *Eur. J. Mech. A Solids* **13**, 93 (1994).
7. M. Jean, *Comput. Meth. Appl. Mech. Eng.* **177**, 235 (1999).
8. L. Brendel, T. Unger and D. E. Wolf, *The Physics of Granular Media* (Wiley-VCH, Weinheim, 2004), p. 325.
9. P. K. Haff, *J. Fluid Mech.* **134**, 401 (1983).
10. S. McNamara and W. R. Young, *Phys. Rev. E* **50**, R28 (1994).
11. A. Mehta, *Granular Matter* (Springer-Verlag, New York, 1994).
12. R. Zallen, *The Physics of Amorphous Solids* (Wiley, New York, 1983).
13. J. P. Hansen and I. R. McDonald, *Theory of Simple Liquids* (Academic Press, New York, 1986).
14. S. Torquato, *Random Heterogeneous Materials* (Springer-Verlag, New York, 2002).
15. A. J. Liu and S. R. Nagel, *Nature* **396**, 21 (1998).
16. G. Combe and J. N. Roux, *Phys. Rev. Lett.* **85**, 3628 (2000).
17. T. Aste and D. Weaire, *The Pursuit of Perfect Packing* (IOP Publishing, New York, 2000).
18. H. C. Andersen, *J. Chem. Phys.* **72**, 2384 (1980).
19. T. Unger *et al.*, *Phys. Rev. E* **65**, 061305 (2002).
20. J. Christoffersen, M. M. Mehrabadi and S. Nemat-Nasser, *J. Appl. Mech.* **48**, 339 (1981).
21. M. R. Shaebani, T. Unger and J. Kertész, *Phys. Rev. E* **76**, 030301(R) (2007).
22. M. R. Shaebani, T. Unger and J. Kertész, *Phys. Rev. E* **78**, 011308 (2008).

23. A. Kolb and B. Dunweg, *J. Chem. Phys.* **111**, 4453 (1999).
24. M. Parrinello and A. Rahman, *Phys. Rev. Lett.* **45**, 1196 (1980).
25. M. P. Allen and D. J. Tildesley, *Computer Simulation of Liquids* (Oxford University Press, New York, 1996).
26. M. R. Shaebani, T. Unger and J. Kertész, *Phys. Rev. E* **79**, 52302 (2009).